makes it difficult to establish good correlations with other South American preceramic phases. Nutting stones, such as recovered from Preceramic Component A, have been reported from both the Talamanca and Boquete phases from Panama, where they were hypothesized to have been used to crush palm nuts (*8*). It is probable that the nutting stone from Provincial was similarly used for processing palm nuts. Ground stone axes from other preceramic assemblages have dates comparable to or slightly later than that obtained from Preceramic Component A, such as the Cerca Grande complex in Brazil dated at 7600 and 7000 B.C. (*9*), the Siches phase in Peru dated between 6000 and 4000 B.C. (*10*), and the Late Las Vegas phase of Ecuador dated between ~6000 and 4600 B.C. (*11*).

The above correlations allow the Orinoco preceramic components to be placed in a provisional chronological framework. The earliest, supported by the radiocarbon date of 7070 B.C., is Preceramic Component A from Provincial, followed by Preceramic Component B. Taking into consideration the similarities with the other flake scraper assemblages noted above, Atures I and II are estimated to date between 7000 and 4000 B.C., with Atures I at the earlier end and Atures II at the later end of the period. Although lacking similar flake tools, Preceramic Component A and Component B are included within Atures I on the basis of their probable contemporaneity. These two components, located away from the Orinoco and containing different tool categories, may represent specialized extractive activities. The termination of Atures II could be later than estimated. The presence of several Barrancoid occupations in the Provincial area dated between 1000 B.C. and A.D. 1 (*3*) suggests that Atures II ended at the latest at ~1000 B.C.

The two preceramic complexes from the Provincial site and the Atures I and II phases from the Culebra site represent early Holocene adaptations to the tropical lowland environment of the Orinoco River. They may be part of a widespread, post-Pleistocene radiation into the tropical lowlands originating from the northern Andean region, given the similarities with tool kits from the Sabana de Bogota. The assemblages, in particular the flake scrapers from the Atures phases, reflect a tool kit designed for the manufacture of items from cane, wood, and bone, materials upon which most of the tropical forest culture's technological repertoire is predicated. These newly defined preceramic components belong to a Tropical Forest Archaic stage (*8*), representing early Holocene adaptations to tropical forest and savanna environments. Documenting the presence of these four preceramic components opens new avenues of inquiry in the archeology of the northern tropical lowlands. It demonstrates a respectable antiquity for the occupation of the Orinoco River valley and suggests that tropical forest-savanna adaptations were effected in the immediate post-Pleistocene period.

REFERENCES AND NOTES

1. C. Evans and B. J. Meggers, *Smithson. Inst. Bur. Am. Ethnol. Bull.* 177 (1960).
2. I. Rouse and J. M. Cruxent, *Venezuelan Archeology* (Yale Univ. Press, New Haven, CT, 1963).
3. W. P. Barse, thesis, Catholic University, Washington, DC (1989).
4. W. Roth, in *Smithson. Inst. 38th Annu. Rep. Bur. Am. Ethnol.* (1924), pp. 27–745.
5. W. R. Hurt *et al.*, *Science* **175**, 1106 (1971).
6. G. C. Urrego, *Investigaciones Arqueologicas en Abrigos Rocosos de Nemocon y Sueva* (Banco de Republica, Bogotá, Colombia, 1979).
7. A. Ranere, in *Proceedings of the First Puerto Rican Symposium on Archeology*, L. Robinson, Ed. (Fundacion Arqueologica, Antropologica, e Historia de Puerto Rico, San Juan, 1976), pp. 103–121.
8. ———, *Peabody Mus. Archeol. Ethnol. Monogr.* **5**, 16 (1980).
9. W. R. Hurt, *Am. Antiq.* **30**, 25 (1964).
10. J. B. Richardson III, in *Variations in Anthropology*, D. W. Lathrap and J. Douglas, Eds. (Urbana Free Library, Urbana, IL, 1973), pp. 199–211.
11. K. E. Stothert, *Am. Antiq.* **50**, 613 (1985).
12. I thank M. Sanoja of the Academia Nacional de Historia in Caracas for support while in the field. I am grateful to B. Meggers, W. Gardner, and M. Thurman for commenting on various drafts of this paper. Fieldwork was supported under National Science Foundation grant BNS-8616324.

19 January 1990; accepted 26 July 1990

Oxygen Isotope Effect and Structural Phase Transitions in La_2CuO_4-Based Superconductors

M. K. CRAWFORD, W. E. FARNETH, E. M. MCCARRON, III,
R. L. HARLOW, A. H. MOUDDEN

The oxygen isotope effect on the superconducting transition temperature (α_o) varies as a function of x in $La_{2-x}Sr_xCuO_4$ and $La_{2-x}Ba_xCuO_4$, with the maximum α_o values ($\alpha_o \geq 0.5$) found for x near 0.12. This unusual x dependence implies that the isotope effect is influenced by proximity to the *Abma* → *P4₂/ncm* structural phase transition in these systems. Synchrotron x-ray diffraction measurements reveal little change in lattice parameters or orthorhombicity due to isotope exchange in strontium-doped materials where $\alpha_o > 0.5$, eliminating static structural distortion as a cause of the large isotope effects. The anomalous behavior of α_o in both strontium- and barium-doped materials, in combination with the previously discovered *Abma* → *P4₂/ncm* structural phase-transition in $La_{1.88}Ba_{0.12}CuO_4$, suggests that an electronic contribution to the lattice instability is present and maximizes at ~1/8 hole per copper atom. These observations indicate a close connection between hole doping of the Cu-O sheets, tilting instabilities of the CuO_6 octahedra, and superconductivity in La_2CuO_4-based superconductors.

ISOTOPE EFFECTS HAVE BEEN WIDELY investigated in the new high transition temperature (T_c) superconductors in order to clarify the role of electron-phonon interactions in the microscopic pairing mechanism (*1, 2*). The demonstration of an isotope effect on T_c played an important role in the development of the Bardeen-Cooper-Schreiffer (BCS) theory of phonon-mediated superconductivity (*1, 2*). In multielement systems such as the high T_c metal oxides, the effect of isotope mass change ΔM_i on the transition temperature ΔT_c can be written as

$$\frac{\Delta T_c}{T_c} = \sum_i \alpha_i \frac{\Delta M_i}{M_i} \tag{1}$$

where the index i is summed over all the lattice sites in the structure. Since it is expected that high-frequency oxygen vibrations make the largest contribution to α, most isotope effect studies in high T_c systems have measured the oxygen partial isotope effect α_o. In general, the measured values of α_o have been greater than zero, but significantly smaller than the BCS limit of $\alpha = 0.5$, and therefore have not been conclusive in determining the importance of phonons in the pairing mechanism (*3, 4*).

An important fact which was not explicitly considered in the earlier high T_c isotope effect measurements is that these materials have complex phase diagrams which exhibit superconductivity over ranges of doping. Isotope effects have typically been measured only for materials with fixed compositions in

---

M. K. Crawford, W. E. Farneth, E. M. McCarron, III, R. L. Harlow, E. I. du Pont de Nemours Co., Wilmington, DE 19880–0356.
A. H. Moudden, Brookhaven National Laboratory, Upton, Long Island, NY 11794, and Laboratoire Leon Brillouin, CEA-CNRS Saclay 91191, Gif sur Yvette, France.

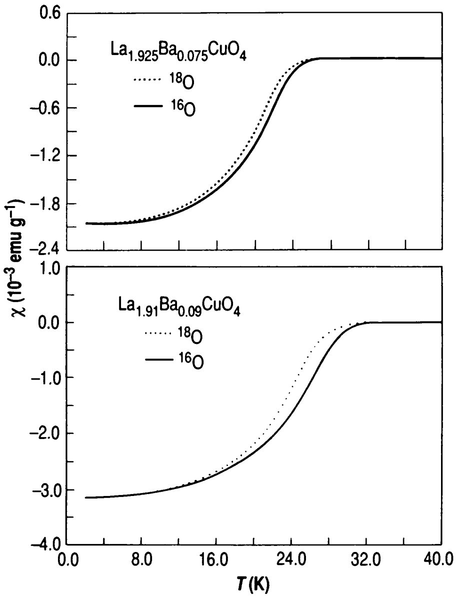

Fig. 1. (**Top**) Meissner data for a ^{16}O, ^{18}O sample pair of $La_{1.925}Ba_{0.075}CuO_4$, $\alpha_o = 0.30$. (**Bottom**) Meissner data for a ^{16}O, ^{18}O sample pair of $La_{1.91}Ba_{0.09}CuO_4$, $\alpha_o = 0.53$.

the optimized regions (highest T_c) of their phase diagrams. The question of whether the isotope effect varies across the phase diagram has not been addressed. We have therefore made a systematic study of the oxygen isotope effect versus x in $La_{2-x}Sr_xCuO_4$ and $La_{2-x}Ba_xCuO_4$. A preliminary report of the results for the $La_{2-x}Sr_xCuO_4$ system has appeared elsewhere (*5*).

A complete description (*6*) of the experimental details for the synthesis, isotope exchange, flux exclusion, and infrared measurements is given elsewhere (*5*). In Table 1 we list the new α_o values, along with other relevant information, for each sample pair studied. Synchrotron x-ray diffraction data were obtained at the National Synchrotron Light Source, Brookhaven National Laboratory, Upton, New York (*7*).

In Fig. 1 we show the Meissner data for $La_{1.925}Ba_{0.075}CuO_4$ and $La_{1.91}Ba_{0.09}CuO_4$ (^{16}O and ^{18}O) samples. In order to obtain α_o values, we apply the following criteria to the Meissner data: (i) The ^{18}O and ^{16}O curves must be parallel or nearly so; (ii) both curves must reach low temperature saturation values so that we may apply the normalization procedure (*8*). In general, in the $La_{2-x}Ba_xCuO_4$ system the superconducting transitions are most narrow at low doping levels, that is, $x \leq 0.09$, and it is for these samples that we obtain the most accurate isotope effect measurements. In the region $0.1 \leq x < 0.15$, the transitions are very broad and we cannot obtain reliable isotope shift data. It is also in this region of the phase diagram that the *Abma*-D_{2h}^{18} [low temperature orthorhombic (LTO) phase in the nomenclature of (*9*)] → $P4_2/ncm$-D_{4h}^{16} [low temperature tetragonal (LTT) phase] phase transition (Fig. 2) is occurring for a large fraction of the sample (*9*). Indications are that the LTT phase is either nonsuperconducting or has suppressed superconductivity relative to the LTO phase. Inclusions of the LTT phase within the superconducting LTO phase will decrease the amount of flux exclusion, and broaden the magnetic transition, as we and others observe (*9*). For $0.15 < x < 0.175$, the Meissner data sharpen and reach a low temperature saturation, which allows determination of isotope shifts with reasonable certainty. However, for $x > 0.175$, we again have difficulty preparing samples that have satisfactory transition profiles.

In Fig. 3 we plot α_o versus x for both $La_{2-x}Ba_xCuO_4$ and $La_{2-x}Sr_xCuO_4$. The Sr data has been extended by three additional x values from that reported by Crawford *et al.* (*5*). The isotope effect in $La_{2-x}Sr_xCuO_4$ is much larger for $x = 0.12$ than $x = 0.15$ (where T_c is maximum), as evident from the data shown in Fig. 4. The value of α_o at $x = 0.15$ is in good agreement with previous measurements (*4*). The general trend we observe, large α_o (0.5 or larger) for x approaching 0.12, but small α_o ($\alpha_o \leq 0.2$) for $x = 0.15$ and 0.175, is similar for both Ba- and Sr-doped systems. The maximum measured values of α_o occur at $x = 0.12$ in $La_{2-x}Sr_xCuO_4$ and at $0.10 \leq x < 0.15$ in $La_{2-x}Ba_xCuO_4$ (Fig. 3). These variations are well correlated with the LTO → LTT phase transition data for $La_{2-x}Ba_xCuO_4$ of Axe *et al.* (*9*). The region of maximum structural instability in that system (highest conversion to LTT) also occurs at $x \cong 0.12$.

Table 1. Summary of isotope data for $La_{2-x}Ba_xCuO_4$ and $La_{2-x}Sr_xCuO_4$ samples [also see (*5*)]. The α_o values are only given for $La_{2-x}Ba_xCuO_4$ samples with x = 0.075, 0.090, 0.100, 0.150, and 0.175. For other values of x, the Meissner transitions are too wide and do not saturate at low temperatures, preventing us from extracting accurate α_o values.

x	T_c (onset)	T_c (midpoint)	ΔT_c	% ^{18}O	$\nu(^{16}O)/\nu(^{18}O)$ (240 cm^{-1})	$\nu(^{16}O)/\nu(^{18}O)$ (500 cm^{-1})	α_o
				$La_{2-x}Ba_xCuO_4$			
0.075	24.0	20.1	0.76	92	1.043	1.051	0.30
0.090	29.3	24.4	1.6	90	1.043	1.050	0.53
0.100	29.2	15.6	1.9	91	1.043	1.058	0.62
0.110	29.1	15.6	. . .	. . .	. . .	. . .	. . .
0.125	29.0	15.4	. . .	. . .	. . .	. . .	. . .
0.150	29.1	22.5	0.6	86	1.030	1.050	0.21
0.175	24.6	16.2	0.29	92	. . .	. . .	0.11
0.200	23.4	13.8	. . .	. . .	. . .	. . .	. . .
				$La_{2-x}Sr_xCuO_4$*			
0.12	29.4	25.4	2.2	92	1.034	1.045	0.78
0.12†	29.1	25.4	2.3	87	1.042	1.055	0.85
0.13	34.4	29.8	2.0	89	1.04	1.053	0.57
0.14	36.9	32.4	0.59	90	1.04	1.05	0.15

*Data for other x values for $La_{2-x}Sr_xCuO_4$ are given in (*5*). †This sample pair was annealed at 700°C for 72 hours. This presumably increases the oxygen context and thereby the doping level to x slightly greater than 0.12, increasing α_o while decreasing T_c. An $x = 0.15$ sample annealed at 700°C for 72 hours had the same α_o value as a sample annealed at 850°C, which is consistent with the essentially constant α_o for $x \geq 0.15$.

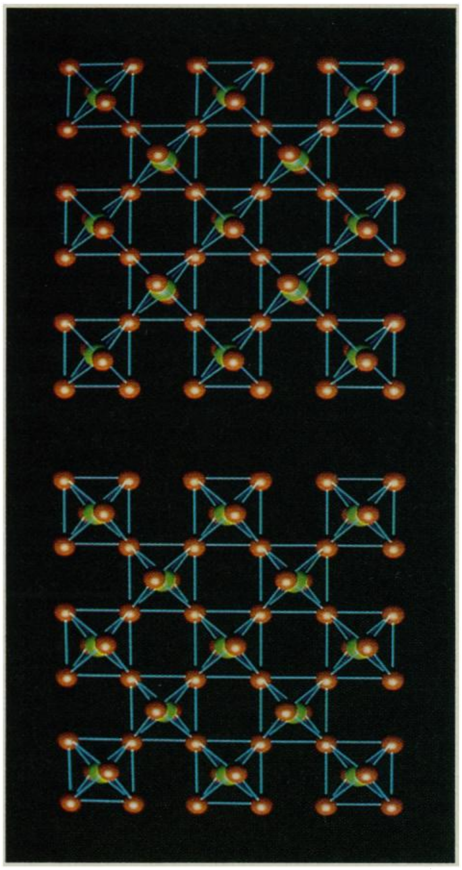

Fig. 2. LTT (**Top**) and LTO (**Bottom**) tilt structures of $La_{1.88}Ba_{0.12}CuO_4$. The *c*-axis is perpendicular to the layer plane. The tilt angles have been exaggerated by a factor of 2 for clarity. In the LTO structure, the octahedra are rotated about the HTT [110] axis. The LTO → LTT transformation is accomplished by a second rotation, of the same magnitude, about the HTT [$1\bar{1}0$] axis. In the LTT structure, the Cu-O layers adjacent to the one shown are rotated about the *c*-axis by 90°.

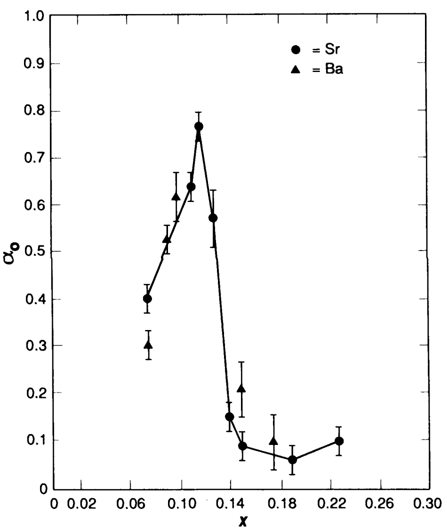

Fig. 3. Oxygen isotope effect (α_o) versus x for $La_{2-x}Ba_xCuO_4$ and $La_{2-x}Sr_xCuO_4$. α_o is defined as $T_c \sim M^{-\alpha_o}$, where M is the (average) oxygen mass.

Thus it seems likely that this phase transition is influencing the isotope effect. This suggests that the structural instability leading to the phase transition in $La_{2-x}Ba_xCuO_4$ is also present in Sr-doped material, and that there may be a connection between the phonons involved in the LTO → LTT phase transition and the occurrence of superconductivity in doped La_2CuO_4.

The relationship between superconductivity and the LTO → LTT phase transition is also apparent in the T_c data. In Fig. 5 we show T_c versus x for $La_{2-x}Sr_xCuO_4$ and $La_{2-x}Ba_xCuO_4$, for both onset and midpoint T_c taken from the magnetization curves. It is apparent that both materials exhibit a minimum in T_c near $x = 0.12$. In $La_{2-x}Ba_xCuO_4$ this has been attributed to the formation of the LTT phase (*9*), in which superconductivity is suppressed. In $La_{2-x}Sr_xCuO_4$, despite the lack of appearance of the LTT phase (discussed below), T_c still exhibits a shallow minimum near $x = 0.12$ [Fig. 5 and (*10*)]. We believe that the minimum in T_c for $La_{1.88}Sr_{0.12}CuO_4$ also arises from proximity to the LTO → LTT lattice instability.

X-ray diffraction structural studies have been performed on several $La_{2-x}Sr_xCuO_4$ samples for three purposes: first, to determine whether the $Sr_{0.12}$ samples undergo any low temperature structural distortion associated with octahedra tilts; second, to see if ^{18}O incorporation produces any lattice distortion (that is, are the ^{16}O and ^{18}O samples in a given pair structurally different?); and finally, to verify, as accurately as possible, that the oxygen contents of the isotope pairs are the same.

In Fig. 6 we show orthorhombicity versus temperature data for isotope pairs of $La_{1.89}Sr_{0.11}CuO_4$ ($\alpha_o = 0.64$) and $La_{1.85}Sr_{0.15}CuO_4$ ($\alpha_o = 0.1$). All samples remain orthorhombic at low temperature, with no indication of a decrease in orthorhombicity for the $x = 0.12$ samples which might signal the approach to LTT symmetry. There is also no observed difference in orthorhombicity, for either value of x, which can be associated with the oxygen mass or oxygen content. We do observe the well-known decrease in HTT → LTO transition temperature and low temperature orthorhombicity resulting from increased Sr concentration (*9*).

In Table 2, we list room temperature and low temperature (~20 K) lattice parameters for a $La_{1.88}Sr_{0.12}CuO_4$ sample pair which was annealed at 700°C in oxygen, rather than at 850°C, our standard temperature for isotope exchange. This pair exhibited a very large isotope effect, $\alpha_o = 0.85$ (Table 1). At room temperature (HTT structure) the ^{18}O sample has, within error, a unit cell volume equal to that of the ^{16}O sample. At 20 K (LTO structure), the ^{18}O unit cell is slightly smaller, with the difference being near the sensitivity limit. We also list in Table 2 the 20 K lattice parameters for a $La_{1.85}Sr_{0.15}CuO_4$ sample pair ($T_c = 38$ K, $\alpha_o = 0.09$). Again the ^{18}O sample has lattice parameters slightly smaller than the ^{16}O sample. These small differences, associated with isotope exchange, imply that the variation of α_o (x) does not originate from differences in oxygen content between members of isotope pairs or from the effect of an isotope-induced structural distortion on a non-phonon coupling mechanism (*11*). The latter conclusion also follows from considering the pressure dependence of T_c. The ^{18}O substitution leads to a small decrease in the low temperature lattice parameters (that is, near T_c), perhaps due to anharmonicity, although the precise origin is unknown. This type of distortion is similar (but not equivalent) to that produced by increased external pressure. ^{18}O substitution decreases T_c, however, whereas application of pressure increases T_c (*12*). Therefore, our structural data lead us to conclude that the isotope effects we measure are not a consequence of the effect of ^{18}O substitution on the static lattice structure, but rather that their origin lies either in the anharmonic lattice dynamics or unusual electronic effects (such as density of state variations) associated with proximity to the LTO → LTT lattice instability.

The sequence of known (*9*) phase transitions in $La_{1.88}Ba_{0.12}CuO_4$ is *I4/mmm* (HTT) → *Abma* (LTO) → *P4₂/ncm* (LTT). Each of these phase transitions involves a rotation of the CuO_6 octahedra, first about the [110] HTT axis and then about the [$1\bar{1}0$] HTT axis (Fig. 2). The primitive unit

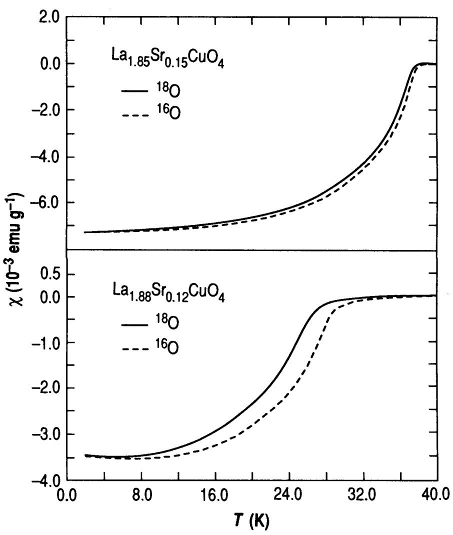

Fig. 4. (**Top**) Meissner data for an ^{16}O, ^{18}O sample pair of $La_{1.85}Sr_{0.15}CuO_4$, $\alpha_o = 0.10$. (**Bottom**) Meissner data for an ^{16}O, ^{18}O sample pair of $La_{1.88}Sr_{0.12}CuO_4$. A magnetic field of 3 G was used. This x value has a large $\alpha_o = 0.77$.

cells double in volume as a result of each transition (Z = 1, 2, and 4 for the HTT, LTO, and LTT structures, respectively). The LTO → LTT transition doubles the periodicity along the c axis. The conventional unit cell parameters are $a \times a \times c$, $\sqrt{2}a \times \sqrt{2}a \times c$, and $\sqrt{2}a \times \sqrt{2}a \times c$ for the HTT, LTO, and LTT structures, respectively (ignoring the small orthorhombic distortion in the LTO structure). This sequence of phase transitions is also known to occur in La_2NiO_4 (*13*), La_2CoO_4 (*14*), and $(CH_3NH_3)_2MCl_4$ (*15*), where M, for example, is Mn or Cd. The HTT → LTO phase transition is expected to be second order based upon symmetry considerations, and the experimental data, for example in La_2CuO_4, are consistent with this expectation (*16*). On the other hand, the LTO → LTT transition is expected to be first order by symmetry (*15*) and appears so from experiment (*9*).

There are other important differences between the HTT → LTO and the LTO → LTT phase transitions. The HTT → LTO phase transition is not accompanied by large changes in transport properties, despite the fact that calculations indicate significant electronic coupling to octahedra tilting phonons in the HTT phase (*17*). In contrast, the LTO → LTT transition exhibits large changes in transport properties (*18*). Furthermore, the HTT → LTO transition temperature smoothly decreases with x (*19*), whereas the LTO → LTT transition occurs only in a narrow region around $x \cong 0.12$. Together, these observations demonstrate a significant electronic coupling to the LTO → LTT lattice instability.

The confinement of the LTO → LTT in-

Table 2. Lattice parameters for $La_{2-x}Sr_xCuO_4$ isotope pairs at 300 K and 20 K. The numbers in parentheses are estimated standard deviations.

	$La_{1.88}Sr_{0.12}CuO_4$ ($\alpha_o = 0.85$)				$La_{1.85}Sr_{0.15}CuO_4$ ($\alpha_o = 0.10$)	
	HTT (T = 300 K)*		LTO (T = 20 K)†		LTO (T = 20 K)‡	
	^{16}O	87% ^{18}O	^{16}O	87% ^{18}O	^{16}O	87% ^{18}O
a (Å)	3.78131(7)	3.78129(7)	5.3245(2)	5.3234(1)	5.3222(1)	5.3214(1)
b (Å)	. . .	. . .	5.3629(2)	5.3626(1)	5.3452(1)	5.3449(1)
c (Å)	13.2240(4)	13.2246(3)	13.1771(6)	13.1754(3)	13.1945(2)	13.1933(3)

*Lattice parameters refined in space group *I/mmm* (D_{4h}^{17}) from positions of 33 reflections. †Lattice parameters refined in space group *Abma* (D_{2h}^{18}) from positions of 15 reflections. ‡Same as † with 30 reflections.

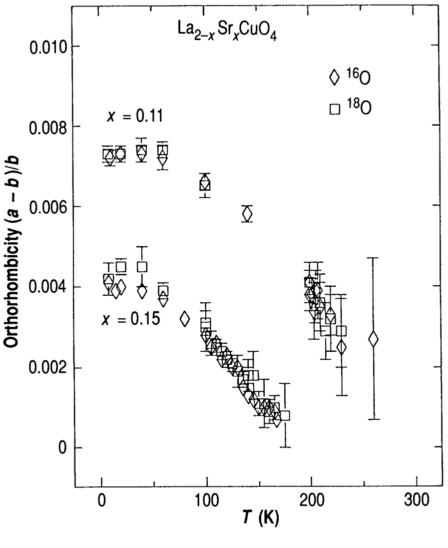

Fig. 6. Orthorhombicity versus temperature for $La_{1.89}Sr_{0.11}CuO_4$ ($\alpha_o = 0.64$) and $La_{1.85}Sr_{0.15}CuO_4$ ($\alpha_o = 0.1$). Note that orthorhombicity is sensitive to the doping (x) value and thus places strong constraints on the relative oxygen contents of a ^{16}O, ^{18}O sample pair (approximately ± 0.002 O^{2-} per formula unit).

stability to a small region of the phase diagram near $x = 0.12$ requires further discussion. There are several examples of insulating isostructural materials which undergo this structural transformation, for example, $La_2NiO_{4+\delta}$ when $\delta \approx 0$ (*20*). This demonstrates that ionic forces are sufficient to produce the instability in the absence of charge carriers. In fact, in undoped La_2CuO_4 the instability is apparently incipient (*16*). The isotope effect measurements, however, imply that the LTO → LTT instability in doped La_2CuO_4 is located at $x = 0.12$ independent of dopant size [Ba^{2+} 1.47 Å; Sr^{2+} 1.31 Å (*21*)]. In order to tie some of these observations together, we propose the following speculative model. The CuO_6 octahedra are intrinsically unstable to tilting distortions. The resulting tilt structures are stabilized by temperature-dependent ionic forces. There is strong interlayer coupling of the octahedra tilting phonons in LTO La_2CuO_4 as demonstrated by the large $Z_3{}^+$ phonon dispersion in the (001) direction (*16*). This coupling will depend upon the interlayer distance, which changes with dopant size or, for example, with the application of external pressure (*22*). The introduction of free charge carriers by doping will modify these ionic forces by (anisotropic) electronic screening, and thereby change the free energy of a particular tilt structure. Interestingly, the LTO → LTT transition has been described (*23*) as a charge density wave (CDW)–coupled distortion, and perhaps the intrinsic ionic instability is supplemented by a lock-in electronic contribution to the Landau free energy at $x = 0.12$. The presence of a commensurate CDW when $x = 0.12$ (~1/8) depends on the Fermi surface topology at that carrier concentration. Angle resolved photoemission spectroscopy is one technique which can yield this information (*24*), and such measurements as a function of x in single crystals of $La_{2-x}(Sr,Ba)_xCuO_4$ would be very interesting. It is possible that in high T_c materials, instabilities between specific (tilt) structures might exist as commensurate or incommensurate functions of hole doping in the Cu-O sheets, and electron-phonon–coupled superconductivity exists near some of these instabilities.

Following this line of reasoning further, if the LTO → LTT phase transition were due to a CDW, then one might expect an energy gap to open at the Fermi surface in the LTT phase. We have looked for a gap by infrared reflectance and find no evidence for one at energies above 30 cm^{-1} (~4 meV). If one assumes a mean field value for this gap (that is, $2\Delta = 3.5\,kT$, where T, the LTO → LTT phase transition temperature, is 70 K), then $2\Delta \approx 160$ cm^{-1}, significantly greater than our low energy measurement limit of 30 cm^{-1}. Thus, clear evidence that the LTO → LTT instability is due to a CDW (*23, 25*) is still lacking, as is an explanation for the suppression of superconductivity in the LTT phase.

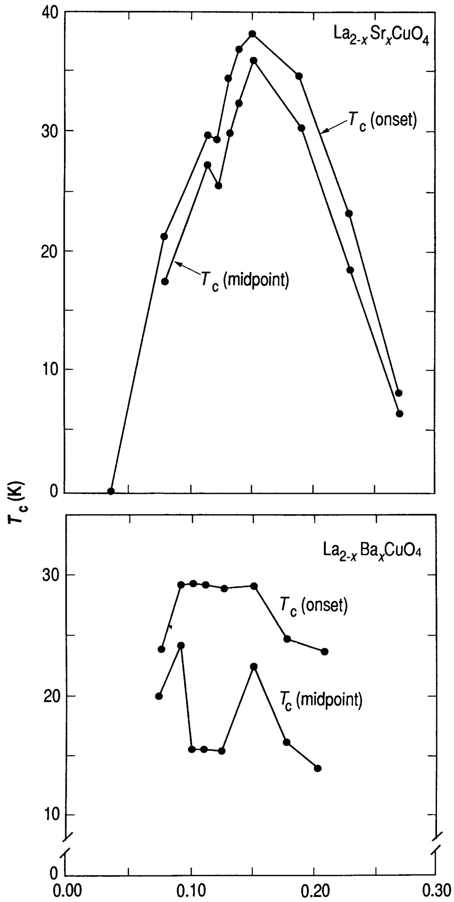

Fig. 5. (**Top**) Superconducting transition temperature T_c (onset and midpoint) versus x for $La_{2-x}Sr_xCuO_4$. (**Bottom**) Superconducting transition temperature T_c (onset and midpoint) versus x for $La_{2-x}Ba_xCuO_4$.

REFERENCES AND NOTES

1. E. Maxwell, *Phys. Rev.* **78**, 477 (1950); C. A. Reynolds, B. Serin, W. H. Wright, L. B. Nesbitt, *ibid.*, p. 487.
2. J. Bardeen, L. N. Cooper, J. R. Schrieffer, *ibid.* **108**, 1175 (1957).
3. S. Hoen *et al.*, *Phys. Rev. B* **39**, 2269 (1989), and references therein; B. Batlogg *et al.*, *Phys. Rev. Lett.* **61**, 1670 (1988); D. G. Hinks, D. R. Richards, B. Dabrowski, D. T. Marx, A. W. Mitchell, *Nature* **335**, 419 (1988).
4. B. Batlogg *et al.*, *Phys. Rev. Lett.* **59**, 912 (1987); T. A. Faltens *et al.*, *ibid.*, p. 915.
5. M. K. Crawford, M. N. Kunchur, W. E. Farneth, E. M. McCarron, S. J. Poon, *Phys. Rev. B* **41**, 282 (1990).
6. A minor modification of the procedure described by Crawford *et al.* (*5*) is that the data reported here were obtained exclusively on powders which were loaded into gelatin capsules for the magnetic susceptibility measurements. The magnetic measurements were made using a Quantum Design SQUID magnetometer operating at a field of 3 G. Synthesis procedures for the $La_{2-x}Ba_xCuO_4$ samples were essentially identical to those of the $La_{2-x}Sr_xCuO_4$ samples described elsewhere (*5*).
7. The powder diffractometer was set up in a high resolution mode with a Si(111) monochromator and a Ge (220) analyzing crystal [D. E. Cox, B. H. Toby, M. M. Eddy, *Aust. J. Phys.* **91**, 117 (1988)]. The wavelength and 2θ offset were determined by refinement of the observed d-spacings of a Si standard. A wavelength of 1.33442(3) Å was used for the $La_{1.88}Sr_{0.12}CuO_4$ samples while 1.22185(3) Å was used for $La_{1.85}Sr_{0.15}CuO_4$. The diffraction

peaks were fit with mixed Lorentzian and Gaussian profiles to obtain accurate 2θ values from which the unit cell dimensions were refined.
8. The normalization procedure involves multiplying the ^{18}O magnetic data by a factor so that the ^{16}O and ^{18}O curves intersect at 2 K. This factor is typically between 1.0 and 1.2. The low temperature magnetic susceptibilities of the ^{18}O samples are always smaller, and we do not understand the origin of the small reduction of the Meissner effect after ^{18}O substitution. There is no apparent correlation of this phenomenon with x.
9. J. D. Axe *et al.*, *Phys. Rev. Lett.* **62**, 2751 (1989); A. R. Moodenbaugh, Y. Xu, M. Suenaga, T. J. Fokerts, R. N. Shelton, *Phys. Rev. B* **38**, 4596 (1988).
10. H. Takagi *et al.*, *Phys. Rev. B* **40**, 2254 (1989).
11. D. S. Fisher, A. J. Millis, B. Shraiman, R. N. Bhatt, *Phys. Rev. Lett.* **61**, 482 (1988).
12. N. Tanahashi *et al.*, *Jpn. J. Appl. Phys.* **28**, L762 (1989).
13. G. H. Lander, P. J. Brown, J. Spalek, J. M. Honig, *Phys. Rev. B* **40**, 4463 (1989).
14. K. Yamada *et al.*, *ibid.* **39**, 2336 (1989).
15. D. M. Hatch, H. T. Stokes, K. S. Aleksandrov, S. V. Misyul, *ibid.*, p. 9282, and references therein.
16. P. Boni *et al.*, *ibid.* **38**, 185 (1988); T. R. Thurston *et al.*, *ibid.* **39**, 4327 (1989); R. J. Birgeneau *et al.*, *Phys. Rev. Lett.* **59**, 1329 (1987).
17. R. E. Cohen, W. E. Pickett, H. Krakauer, *Phys. Rev. Lett.* **62**, 831 (1989).
18. M. Sera *et al.*, *Solid State Commun.* **69**, 851 (1989).
19. R. M. Fleming, B. Batlogg, R. J. Cava, E. A. Rietman, *Phys. Rev. B* **35**, 7191 (1987).
20. D. E. Rice, M. K. Crawford, D. J. Buttrey, W. E. Farneth, *ibid.*, in press.
21. R. D. Shannon and P. S. Gumerman, *Acta Crystallogr.* **A32**, 751 (1976).
22. N. Yamada, M. Oda, M. Ido, Y. Akajima, K. Yamaya, *Solid State Commun.* **70**, 1151 (1989).
23. S. Barisic and J. Zelenko, *ibid.* **74**, 367 (1990).
24. J. C. Campuzano *et al.*, *Phys. Rev. Lett.* **64**, 2308 (1990), and references therein.
25. Y. Okajima, K. Yamaya, N. Yanada, M. Oda, M. Ido, *Solid State Commun.* **74**, 767 (1990).

26. The authors thank W. Dolinger, D. Groski, R. J. Smalley, and M. W. Sweeten for technical assistance. They also thank M. N. Kunchur and V. J. Emery for helpful discussions, D. E. Cox for help with the synchrotron measurements, and J. Calabrese for producing Fig. 2. We are particularly grateful to J. D. Axe for numerous discussions, help obtaining the data in Fig. 6, and useful comments on this manuscript. We also acknowledge valuable comments by the referees. Research carried out (in part) at the National Synchrotron Light Source, Brookhaven National Laboratory, which is supported by the U.S. Department of Energy, Division of Materials Sciences and Division of Chemical Sciences.

6 August 1990; accepted 11 October 1990

Realized Reproductive Success of Polygynous Red-Winged Blackbirds Revealed by DNA Markers

H. Lisle Gibbs,* Patrick J. Weatherhead, Peter T. Boag, Bradley N. White,† Lisa M. Tabak, Drew J. Hoysak

Hypervariable genetic markers, including a novel locus-specific marker detected by a mouse major histocompatibility complex probe, reveal that multiple paternity is common in families of polygynous red-winged blackbirds (*Agelaius phoeniceus*). Almost half of all nests contained at least one chick resulting from an extra-pair fertilization, usually by a neighboring male. Genetically based measures of reproductive success show that individual males realize more than 20% of their overall success from extra-pair fertilizations, on average, and that this form of mating behavior confounds traditional measures of male success. The importance of alternative reproductive tactics in a polygynous bird is quantified, and the results challenge previous explanations for the evolution of avian polygyny.

An important controversy in studies of avian mating systems is the degree to which observed social relationships of breeding males and females accurately predict patterns of gene transfer across generations (*1*). The observation of copulations between individuals not paired with each other (*2*) and parentage analyses using allozymes (*3*) imply a significant lack of congruence between the behavioral and genetic mating systems of many species and argue that alternative reproductive tactics such as extra-pair fertilizations by males and egg-dumping by females may be important components of individual reproductive success (*4*). If significant, such alternative reproductive behaviors would also raise serious questions about traditional measures of reproductive success used in studies of avian mating systems (*5*).

Theory (*6*) suggests that extra-pair fertilizations (EPFs) may be particularly important sources of male success in polygynous birds like the red-winged blackbird (*Agelaius phoeniceus*) where males provide little parental care. In this species, field experiments have shown that females nesting on the territories of vasectomized males often produced fertile eggs (*7*), and there is evidence that nonterritorial "floater" males are capable of fertilizing females (*8*). We used a combination of traditional and novel hypervariable genetic markers to assess the extent of extra-pair fertilizations in families of red-winged blackbirds and to identify the males responsible. Our results show that some males gain a substantial portion of their reproductive success through EPFs and provide a detailed analysis of realized male and female reproductive success in a natural population of a polygynous bird. They also demonstrate that EPFs severely confound traditional measures of male success and hence call into question previous tests of explanations for the evolution of polygyny in these birds (*9*).

To study parentage in wild blackbirds, we collected blood samples from adults and 6-day-old nestlings from one low-density (0.1 territorial males per hectare) and two high-density (0.4 males per hectare) marshes near the Queen's University Biology Station, Chaffey's Lock, Ontario, in 1986. We successfully collected samples from 75% (21 of 28) of all territorial males in these three marshes and from all chicks in 90% (36 of 40) of nests on the territories of sampled males that had nestlings old enough to be bled. In total the 36 families we sampled consisted of 111 nestlings, 21 putative male, and 31 putative female parents; for 31 of these families we captured both male and female parents, whereas for five nests we only had samples from the presumed male parent (*10*).

For parentage analyses we followed procedures described by Seutin *et al.* (*11*) to extract DNA from the samples and used Southern Blot techniques to carry out pedigree analyses on the families using two types of hypervariable DNA probes. First, a mouse class II major histocompatibility complex (MHC) cDNA probe from the I-alpha locus (*12*) that hybridizes to a locus-specific hypervariable region in the blackbird genome; second, two multi-locus mini-satellite probes, Jeffreys 33.15 (*13*) and the M2.5 repetitive sequence from the *per* gene in mice (*14*). The MHC probe (*15*) detects restriction fragment length polymorphisms in Eco RI–cut genomic DNA that have the genetic characteristics of a single hypervariable locus with many co-dominant alleles ($n = 36$) at low frequencies (mean allele frequency = 2.2%). As a result the probability of false inclusion (*16*) for this locus in blackbirds equals 0.07, which is equivalent to that of many human single locus variable number of tandem repeat (VNTR) markers (*17*). Both mini-satellite probes have been used in parentage analyses of wild birds (*18, 19*); each detects complex individual-specific band patterns in blackbirds (Fig. 1).

Our approach was to use both types of

H. L. Gibbs, P. T. Boag, L. M. Tabak, B. N. White, Department of Biology, Queen's University, Kingston, Ontario, Canada K7L 3N6.
P. J. Weatherhead and D. J. Hoysak, Department of Biology, Carleton University, Ottawa, Ontario, Canada K1S 5B6.

---

*To whom correspondence should be addressed.
†Present address: Department of Biology, McMaster University, Hamilton, Ontario L8S 4K1.